Planetary and Space Science 177 (2019) 104690

Contents lists available at ScienceDirect

Planetary and Space Science

journal homepage: www.elsevier.com/locate/pss

Three-dimensional imaging of crack growth in L chondrites after high-velocity impact experiments

Tatsuhiro Michikami [a,*], Axel Hagermann [b], Akira Tsuchiyama [c,d], Hirotaka Yamaguchi [e], Terunori Irie [a], Keita Nomura [a], Osamu Sasaki [f], Michihiko Nakamura [g], Satoshi Okumura [g], Sunao Hasegawa [h]

[a] Faculty of Engineering, Kindai University, Hiroshima Campus, 1 Takaya Umenobe, Higashi-Hiroshima, Hiroshima, 739-2116, Japan
[b] Department of Biological and Environmental Sciences, University of Stirling, FK9 4LA, United Kingdom
[c] Research Organization of Science and Technology, Ritsumeikan University, 1-1-1 Nojihigashi, Kusatsu, Shiga, 525-8577, Japan
[d] Guangzhou Institute of Geochemistry, Chinese Academy of Sciences, 511 Kehua Street, Wushan, Tianhe District, Guangzhou, 510640, China
[e] Division of Earth and Planetary Sciences, Graduate School of Science, Kyoto University, Kitashirakawa Oiwake-cho, Sakyo-ku, Kyoto, 606-8052, Japan
[f] Division of GeoEnvironmental Science, Department of Earth Science, Graduate School of Science, Tohoku University, Aramaki Aoba-ku, Sendai, 980-8578, Japan
[g] Department of Earth Science, Graduate School of Science, Tohoku University, Aramaki Aoba-ku, Sendai, 980-8578, Japan
[h] Institute of Space and Astronautical Science, Japan Aerospace Exploration Agency, Sagamihara, Kanagawa, 252-8510, Japan

ARTICLE INFO

Keywords:
Crack growth
Chondrules
L chondrite
X-ray microtomography
Laboratory impact experiments

ABSTRACT

Small asteroids such as Itokawa are covered with an unconsolidated regolith layer of centimeter-sized or smaller particles. There are two plausible formation mechanisms for regolith layers on a sub-kilometer-sized asteroid: (i) fragments produced by thermal fatigue by day-night temperature cycles on the asteroid surface and (ii) impact fragment. Previous studies suggest that thermal fatigue induces crack growth along the boundary surface of the mineral grain while impact phenomena may induce crack growth regardless of the boundary surface of the mineral grain. Therefore, it is possible that the crack growth within a mineral grain (and/or a chondrule) differs depending on the crack formation mechanism, be it thermal fatigue or an impact.

In order to investigate how mineral grains and chondrules are affected by impact-induced crack growth, we fired spherical alumina projectiles (diameter ~1 mm) into 9 mm side length cubic targets of L chondrites at a nominal impact velocity of 2.0 km/s. Before and after the six successful impact experiments, the cracks within mineral grains and chondrules in the respective targets are examined using X-ray microtomography at a resolution with the voxel size of 9.0 μm. The results show that most cracks within chondrules and troilite (FeS) grow regardless of the boundary surfaces of the grains while most cracks within ductile Fe-Ni metal grow along the boundary surfaces of the grains. This may indicate that crack growth is largely affected by the strength of mineral grains (and/or chondrules). From the experimental results and the fact that the shapes of polymineralic and monomineralic particles from Itokawa are similar, we conclude that the Itokawa particles have not been produced by thermal fatigue but instead are likely to be impact fragments, as described in previous papers (Tsuchiyama et al., 2011, 2014; Michikami et al., 2018).

1. Introduction

Hayabusa was the first spacecraft to explore a sub-kilometer-sized asteroid, Itokawa (e.g. Fujiwara et al., 2006; Saito et al., 2006). Such small asteroids are covered with an unconsolidated regolith layer of centimeter-sized or smaller particles (Yano et al., 2006; Tsuchiyama et al., 2011, 2014). In general, the regolith layers on asteroids of a certain size are considered to be the products of the fragments ejected from the surface by meteoroid impacts (e.g. Housen et al., 1979). However, the formation mechanism of regolith layers on a sub-kilometer-sized asteroid is only poorly understood. For instance, before the arrival of the Hayabusa spacecraft at asteroid Itokawa, most scientists thought that there would be only a few boulders on the surface of such a sub-km sized asteroid because almost all impact fragments were generally considered to have escaped from an asteroid due to its extremely low gravity (e.g. Housen et al., 1979).

* Corresponding author.
E-mail address: michikami@hiro.kindai.ac.jp (T. Michikami).

https://doi.org/10.1016/j.pss.2019.07.005
Received 20 March 2019; Received in revised form 10 June 2019; Accepted 8 July 2019
Available online 11 July 2019
0032-0633/© 2019 The Authors. Published by Elsevier Ltd. This is an open access article under the CC BY license (http://creativecommons.org/licenses/by/4.0/).

Delbo et al. (2014) claimed that day-night temperature cycles on the surface induce thermal fatigue and that this is the dominant process governing regolith generation on small asteroids. In other words, cracks in rocks occur and propagate due to thermal contraction and expansion. In thermal fatigue, amplification of stress occurs at surface-parallel boundaries between adjacent mineral grains as a result of the difference in thermoelastic behavior between adjacent grains (Molaro et al., 2015). Thus, the boundary surfaces of mineral grains (and/or chondrules) may affect the shapes of the fragments produced by thermal fatigue. On the other hand, Tsuchiyama et al. (2011, 2014) and Michikami et al. (2018) suggested that Itokawa regolith particles recovered by the Hayabusa spacecraft are not the products of thermal fatigue but impact fragments on the asteroid surface because their particle shape distribution is similar to the shape distribution of analog impact fragments. In particular, Michikami et al. (2018) concluded from their impact experiments that neither petrographic textures nor crystal grain boundaries significantly affect the shapes of the impact fragments. Therefore, it is possible that the crack growth within mineral grains and chondrules differ depending on the crack formation mechanism, be it thermal fatigue or an impact.

Assuming that Hayabusa's Itokawa particles are impact fragments, one open question is how these fine regolith particles accumulated on the surface of a sub-kilometer-sized asteroid. Itokawa's bulk density is low ($1950 \pm 140\,kg/m^3$; Abe et al., 2006) and its bulk porosity is high (~40%; Abe et al., 2006) compared with ordinary chondrite meteorites (e.g. Medvedev et al., 1985) and other S-type asteroids such as Ida and Eros (e.g. Britt et al., 2002). This suggests that the material strength of Itokawa is low (e.g. Michikami et al., 2008). In that case, a large amount of ejecta tends to have lower velocities as indicated by laboratory impact experiments (e.g. Michikami et al., 2007) and can thus accumulate on the surface. Thus, as one of the formation mechanisms, it is highly likely that the regolith particles on a sub-kilometer-sized asteroid are impact fragments.

Past laboratory impact experiments on analog targets for asteroid materials have focused on the size and/or velocity distributions of fragments (e.g. Fujiwara et al., 1977; Nakamura and Fujiwara, 1991; Michikami et al., 2007). However, there have been no laboratory experiments on a chondrite target to investigate the cracks generated by impacts. Besides, although the properties of meteorites such as their mineralogy, petrology, and chemical and isotopic compositions have been extensively studied (e.g. Mikouchi et al., 2001: Friedrich et al., 2008: Righter et al., 2015), data on the physical properties of mineral grains and chondrules are sparse. Thanks to recent developments in X-ray microtomography, a powerful nondestructive method for obtaining the three dimensional structure of samples with micron or submicron spatial resolution, we are now able to observe the crack distribution of a chondrite (e.g. Friedrich and Rivers, 2013).

In this study, we carried out, impact experiments into 9 mm side length cubic targets of L5 chondrites in order to investigate how mineral grains and chondrules as constituents of the chondrite are affected by impact-induced crack growth. Before and after the impact experiments, the cracks within the respective targets are examined using X-ray microtomography at Tohoku University Museum, Japan (Okumura and Sasaki, 2014).

The crack growth within a grain (and a chondrule) is considered to be influenced by the strength of the grain and the degree of shock loading by the impact. It is difficult to measure the strength of a grain as constituents of the chondrite because we cannot extract an intact grain only. In this paper, in order to investigate the influence of the strength of a grain (and a chondrule) to the crack growth within the grain, we measure chondrules, troilite (FeS), Fe-Ni metal, and aggregates of troilite and Fe-Ni metal. We will abbreviate the collective name to CTMA, and call these grains CTMA grains.

CTMA grains can be expected to vary in strength. The relationship between crack growth within CTMA grains and the degree of shock loading by impact is examined taking the distance from impact point into account (see section 4.3).

To be more precise, as a chondrule consists of several mineral grains, the strength of a chondrule is generally considered to depend largely on the texture type (e.g. Nelson and Rubin, 2002). Thus, it should be kept in mind that the crack growth within a chondrule is likely to differ depending on the texture type. However, this paper tries to provide the first step towards a better understanding of the relationship between CTMA grains and fracture mechanism in ordinary chondrites. The research described here is intended to constrain current interpretations of the formation of regolith particles on small asteroids such as Itokawa.

2. Target samples before impact experiments

2.1. Target properties

The samples used as targets are L5 chondrites (Sayh al Uhaimir 001 (SaU 001), Oman), with shock stage S2 and weathering scale W1 (Meteorite Bulletin Database: https://www.lpi.usra.edu/meteor/). The material is identical to the samples used by Michikami et al. (2018). Target bulk density is $3400\,kg/m^3$, the same as Itokawa regolith particles (Tsuchiyama et al., 2011). Several samples were reserved to measure their physical properties and investigate their petrographic textures. The compressional wave velocity is 6.6 km/s (Michikami et al., 2018), similar to the values found in L and LL chondrites (Yomogida and Matsui, 1983).

Note that, because the Itokawa regolith samples are more similar to LL5/6 chondrites, LL5 or 6 chondrites may be suitable as analogue material of Itokawa rather than the L5 chondrites used in the experiments. The major difference between LL and L chondrites is the metal content. The abundance of metal in L chondrites is slightly higher than that in LL chondrites, reflecting their slightly lower abundance of total iron and higher proportion of metallic iron, although the bulk chemical composition of L chondrites is roughly similar to LL chondrites. According to Hutchison (2004), the modal abundance of metal in LL4-6 chondrites and L4-6 chondrites are ~2 and <5 vol%, respectively. Considering the physical properties of chondrites for crack growth, we think that the difference between LL5/6 and L5 chondrites is comparatively small compared with the bias of sample targets due to their heterogeneity at the sample scales, the degree of shock and thermal metamorphisms experienced by the chondrites. In addition, it is difficult to obtain samples of LL5/6 chondrites in good condition because they are rare. Thus, in the experiments, we used the L5 chondrites of SaU 001 as target materials instead of LL5/6 chondrites.

Fig. 1 shows a scanning electron microscope (SEM) image of a thin section of a typical sample of the target material. The sample is primarily composed of olivine and pyroxene with different grain sizes as crystals in chondrules, recrystallized matrix and mineral fragments. The brightest grayscale corresponds to troilite (FeS) and/or Fe-Ni metal. Various grayscales in silicate grains can be observed. The silicate materials with Fe-rich materials appear to be slightly brighter (e.g. Friedrich and Rivers, 2013).

2.2. X-ray microtomography

The L5 chondrites adopted were cut into six cubes with 9 mm side length and used as targets for impact experiments. The target size was chosen to obtain resolutions with the voxel size of 9.0 μm, which is high enough to identify chondrule shapes and cracks within the sample using X-ray microtomography. Before and after the impact experiments, these target samples were imaged using X-ray beam of 200 kV and 200 μA (ScanXmate-D180RSS270) at Tohoku University Museum, Japan. The advantage of X-ray microtomography is that one can obtain three-dimensional sample shapes and petrographic textures using quantitative absorption contrast (Tsuchiyama et al., 2005; Okumura and Sasaki, 2014) with μm spatial resolution of the samples. Each target was set on a styrofoam sheet attached to a cylindrical stand. CT images were obtained using 2000 projection images (0.18°/projection). Successive CT images

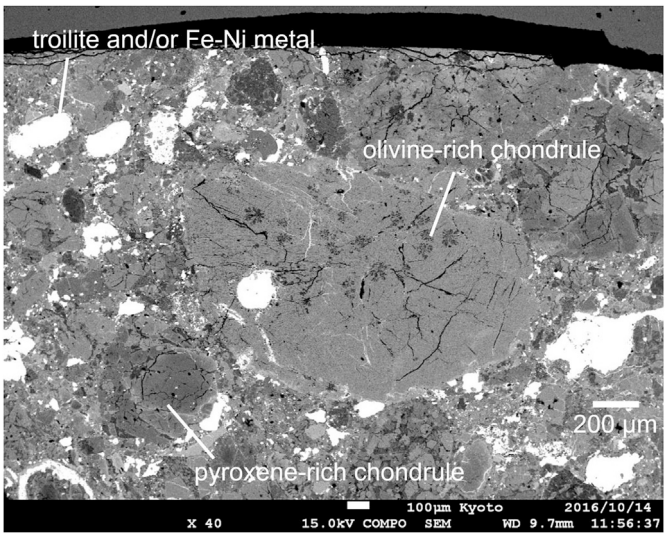

Fig. 1. Back-scattered SEM image (JEOL JSM7001F) of a thin section of a typical L5 chondrite target sample (Sayh al Uhaimir 001 meteorite, Oman). The brightest grayscale corresponds to troilite (FeS) and/or Fe-Ni metal. Various grayscale in silicate grains can be observed. The silicate materials with Fe-rich compositions appear to be brighter. For instance, the largest olivine-rich chondrule in the middle of the figure is slightly brighter than the pyroxene-rich ones located to the bottom left of the figure. Several cracks (black streaks) are observed, especially in these chondrules. In addition, the apparent white streaks are often seen in this sample (these are seen in W1 meteorites). The apparent white streaks are originally cracks and are the products of the terrestrial alteration such as water and oxygen attack. Relatively fine crystals of plagioclase and other minor phases are also present in the recrystallized matrix.

of different slices through the particles were then stacked to obtain their 3-D structure.

The image analysis software ImageJ (a free, open-source image processing program; "https://imagej.nih.gov/ij/") was used for 3-D CT image analysis. A solid object was extracted three-dimensionally by binarization of the CT images as individual particles. The binarization thresholds were determined by eye based on the CT images of each data set. The volume of the chondrules was somewhat changed by the threshold value. The corresponding error will be discussed later.

Fig. 2 shows two typical tomograms of chondrites before the impact experiment examined at resolutions with 9.0 μm/voxel. The features mentioned in Fig. 1 are seen: various grayscales in silicate grains, the brightest grayscale is Fe-Ni metal and the slightly darker material is troilite (Fig. 2(a)), as well as apparent white streaks (Fig. 2(b)) which are originally cracks that have become small oxide veins by being filled with terrestrial weathering products. Air around the sample appears darkest. Our L chondrite samples are 60–80% occupied by chondrules. As L5 chondrites, the samples have experienced significant degrees of thermal metamorphism. In general, chondrules are divided into groups of type I and II (e.g. Villeneuve et al., 2015). Type I chondrules have almost spherical shapes and appear to be darker because of a deficiency in Fe. Type II chondrules, on the other hand, have various shapes and appear to be gray because of abundant Fe. Our samples contain numerous type II chondrules. White or light gray contours are often seen at the rims of some type I chondrules. In chondrules, we only measure crack growth within type I chondrules because it is difficult to distinguish between type II chondrules and the remaining recrystallized matrix due to the low contrast between these materials. Type I chondrules with a deficiency in Fe may be suitable to investigate crack growth as an analog material of Itokawa particles because the Itokawa particles are more similar to LL5/6 chondrites with a deficiency in Fe.

In addition to type I chondrules, by comparison, we also measure crack growth within troilite, Fe-Ni metal and their aggregates as mentioned before (collective name: CTMA). When distinguishing between troilite and Fe-Ni metal, it is necessary to widen the range of grayscale values. In order to measure CTMA grains, we need to change the dynamic range of the image processing. The wide grayscale range in Fig. 2(a) is suitable for distinguishing between troilite and Fe-Ni metal. On the other hand, the narrow grayscale range in Fig. 2(b) is suitable for measuring type I chondrules but not suitable for distinguishing between troilite and Fe-Ni metal because of their brightness saturation.

Before the laboratory impact experiments, at a resolution with 9.0 μm/voxel, obvious large cracks shown in darkest and voids cannot be observed (although smaller and thinner cracks below the imaging resolution level may exist). After the laboratory impact experiments, we focus our observations on CTMA grains with an impact-induced crack. To visualize the crack growth in CTMA grains, we produced three-dimensional images of each cracked CTMA grain using ImageJ.

3. Impact experimental method

The impact experiments for cubic ($9 \times 9 \times 9$ mm) targets of L5 chondrites were performed using a two-stage light-gas gun with a split-type nylon sabot (Kawai et al., 2010) at the Institute of Space and Astronautical Science, Japan Aerospace Exploration Agency (ISAS, JAXA). The targets are set up next to each other, and are attached to an aluminium sheet using double sided tape, as shown in Fig. 3. The reason for putting the targets next to each other is to enlarge the target's area on

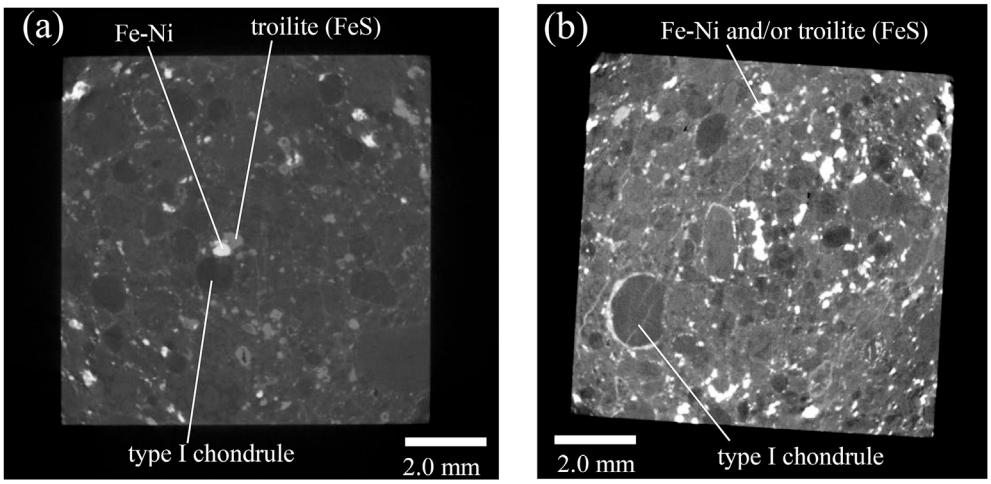

Fig. 2. Two typical tomograms of L5 chondrite samples [(a)#6_XY0684 and (b) #5_XY0785] adopted before the impact experiments at resolutions of 9.0 μm/voxel. Typical Fe-Ni metal, troilite and type I chondrules are shown for each figure, and are measured by changing the dynamic range of the image processing. (a) Wide range of grayscale values, which is adopted to measure Fe-Ni metal and troilite (FeS). Fe-Ni metal is brightest, the slightly darker material is troilite and type I chondrules are darkest. (b) Narrow grayscale range, which is adopted to measure type I chondrules. The darkest material is type I chondrule material. Fe-Ni metal and/or troilite are brightest. In this study, no type II chondrules are measured because it is difficult to distinguish between a type II chondrule and surrounding matrix due to the low contrast between these materials.

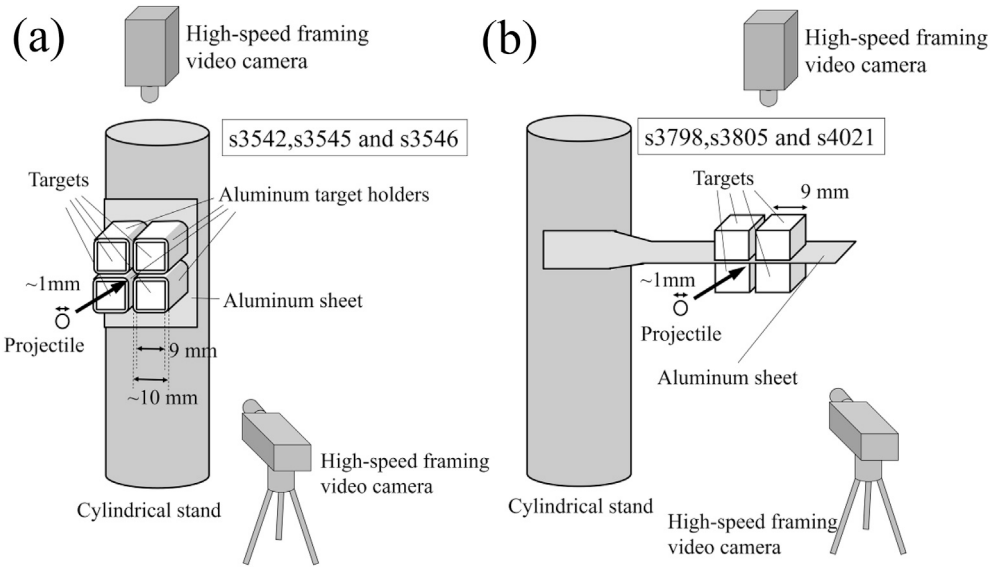

Fig. 3. Configuration of experimental setup. (a) Targets with aluminum target holders. (b) Targets without target holders. The high-speed framing cameras are oriented to view the collision breakup through the side and top windows of the chamber. A cardboard box ($59 \times 56 \times 45\ cm^3$) surrounding the targets and the cylindrical stand was put on the floor of the chamber.

the impact side. In the experiments, it is very difficult to fire a projectile accurately at a 9 mm cubic target because the area exposed on the impact side is very small and the trajectories of the projectiles are not stable enough in the experimental setup.

In all runs, spherical alumina projectiles (diameter ~1.0 mm and mass 0.0027 g and 0.0030 g) were fired perpendicularly into the target surface at a nominal impact velocity of 2.0 km/s (Table 1). The whole system was mounted in a vacuum chamber (approximately $1 \times 1 \times 2\ m^3$ in size) with acrylic resin windows. The ambient pressure in the chamber was less than 30 Pa. A cardboard box ($59 \times 56 \times 45\ cm^3$) was put on the floor of the chamber to prevent the destruction of the largest fragments during secondary collisions with the surface of the chamber. Impact velocities were obtained from the passage time of the projectile between two laser beams.

The experiments were carried out with two different setups. In the first setup of shot s3542, s3545 and s3546 (Fig. 3(a)), each target was enclosed in an aluminum target holder with the front surface fully exposed on the impact side, in order to protect each target from the ejecta and the shock wave from its neighbor broken by the impact. The target holders were made by bending a 0.5 mm thick aluminum sheet, resulting in narrow gaps between the target sides and the target holder; it was only the edges of each target and the surface opposite the impact point that were in contact with the target holder. Due to the resulting increase in target surface, most projectiles hit one of the four targets surfaces. The aluminum sheet with the targets was set on a cylindrical stand. Two high-speed framing cameras were oriented to view the collisional breakup through the side and top windows of the chamber. The fields of view of the two cameras were approximately $10 \times 7\ cm^2$ (side camera) and $25 \times 20\ cm^2$ (top camera), respectively. The framing rate of the cameras was set to 125,000 frames/sec.

In the second setup, used for shots s3798, s3805 and s4021 (Fig. 3(b)), we removed the aluminum target holders. The four targets without aluminum target holder were jointly held in another aluminum sheet by double sided tapes, creating a narrow opening space between targets. The end of the aluminum sheet was set on a cylindrical stand. These targets were oriented with the front surface fully exposed on the impact side. The setup of two high-speed framing cameras was as before.

After each impact, we collected all fragments in the cardboard box and measured the three-dimensional structures of the largest fragment using X-ray microtomography (As an exception, in shot s3546, the second, third and fourth-largest fragments are also measured). With the second setup, we also re-measured the intact targets located adjacent to those broken by the impact. We did not identify any cracks within the intact target samples, although the adjacent, broken, target was heavy fractured. Thus, we assume that the influence of the ejecta and the shock wave from the broken target on its neighbors is negligible. Moreover, we also carried out impact experiments for basalt targets in order to investigate the difference in experimental results between targets with and without target holders (see Appendix A). The result suggests that the difference is negligible because the space distributions of the fracture surfaces are similar.

Table 1
Target properties and the experimental results in the order of decreasing the ratio of mass of largest fragment to initial target mass (M_l/M_t).

Shot number	Target number	Target holder	Impact velocity [km/s]	Projectile mass [g]	Initial target mass, M_t [g]	Largest fragment mass, M_l [g]	M_l/M_t [%]	Distance between impact point and center of the target [mm]	Observed number of cracks for each constituent mineral			
									Chondrules	Troilite (FeS)	Aggregates of troilite(FeS) and Fe-Ni metal	Fe-Ni metal
s3542	#1	Yes	1.96	0.0027	2.480	2.470	99.6	5.4 ± 0.5	3	0	0	3
s3545	#5	Yes	1.98	0.0027	2.520	2.329	92.4	4.3 ± 0.5	7	11	6	12
s3805	#3	No	1.97	0.0030	2.472	1.945	78.7	4.4 ± 0.5	9	0	1	2
s3546	#2	Yes	1.95	0.0027	2.483	1.671	67.3	4.2 ± 0.5	0	6	3	3
s3798	#4	No	1.86	0.0030	2.474	1.073	43.4	2.0 ± 0.5	8	0	0	3
s4021	#7	No	2.06	0.0030	2.477	0.897	36.2	1.0 ± 0.5	0	0	0	4

4. Results

4.1. Degree of fragmentation

As mentioned above, the trajectories of the projectiles are not stable in the experimental setup and thus the impact point deviated from the center of the target surface when the projectiles hit the target. Consequently, we observed a wide range of degrees of target fragmentation, ranging from a chip off the edge to catastrophic disruption. In Fig. 4, the largest fragments of the L5 chondrite targets after impacts are shown in order of the degree of fragmentation. As an indicator of target fragmentation, the ratios of the mass of the largest fragment to the initial target mass (M_l/M_t) are given together with the respective shot number. M_l/M_t is large when only the edge is chipped and/or impact cratering occurs, and is small when catastrophic disruption occurs. The value of M_l/M_t appears to decrease with decreasing distance between the impact point and the center of target surface (Table 1).

4.2. Fracture surfaces and cracks in the largest fragments

We observed the largest fragment shape and distribution of cracks in each shot. Typical tomograms of the largest fragments after impact are shown in Fig. 5 and corresponding illustrations of the main cracks within the largest fragments shown in Fig. 5 are given in Fig. 6. In this study, the terms of "fracture surface" and "crack" refer to the new surface of the largest fragment and the new narrow gap within the largest fragment, originating from the impact, respectively. Overall, the fracture surfaces of the largest fragments are seen near the corner of the original target, and the cracks are also seen parallel to the original target surface in addition to ones near the corner of the original target. The fracture surfaces and the cracks are likely to be produced by rarefaction waves (reflection waves) that originated from the corners, edges or surfaces of the original targets. We give a description for each shot as follows.

s3542 (#1) with target holder

The corner of the target is chipped. A part of the impact energy is consumed by the target holder, which is bend modification near the corner. Cracks are observed parallel to the fracture surface.

s3545 (#5) with target holder

A side of the target is broken. Again, the target holder consumed part of the impact energy as it was bent near the impact. Several cracks are observed parallel and perpendicular to the fracture surface.

s3805 (#3) without target holder

More than half of the target surface is broken. A few cracks are observed parallel to the original target surface.

s3546 (#2) with target holder

A few corners of the target are broken. A part of the impact energy is consumed largely by deformation of the target holder near the impact point. The tomogram contains the second (top left in the figure), third (lower right) and fourth largest fragments (center left). In the second largest fragment, several small cracks are observed parallel to the fracture surface.

s3798 (#4) without target holder

The upper half of the target is heavily broken. Parallel to the target surface, a few cracks are observed.

s4021 (#7) without target holder

More than half of the target of the impact side was heavily broken. Several cracks are observed parallel to the target surfaces and perpendicular to the fracture surface.

In addition to the above descriptions for each shot, we also investigate the relationship between the fracture surfaces (and/or crack growth) and the original large cracks before the impact. Note that the original large cracks in this study are apparent thick cracks and apparent white streaks which are originally cracks observed by X-ray microtomography at resolutions with 9.0 μm/voxel. We do not take into account smaller and thinner cracks below the imaging resolution level although they likely exist.

Three-dimensional imaging data taken before and after the impact experiments are compared. Most fracture surfaces and cracks appear to be independent of the original cracks. However, a few cases of fracture surfaces and cracks resulting from original cracks are observed (Fig. 7). The fracture surfaces resulting from the original cracks are observed for shot s3545 and s3805. The fracture surfaces can be traced back to features that originally used to be cracks. Crack growth of existing cracks is observed for shot s3545 and s3798. These images show the original cracks grow widely. Thus, the influence of the original crack on fracture surface and crack growth cannot be ruled out. However, the influence is considered to be small because almost all fracture surfaces and the cracks are likely to be produced by rarefaction waves (reflection waves) that originated from the corners, edges or surfaces of the targets as mentioned above (as another possibility, the smaller and thinner cracks below the CT imaging resolution level may influence the fracture surface and crack

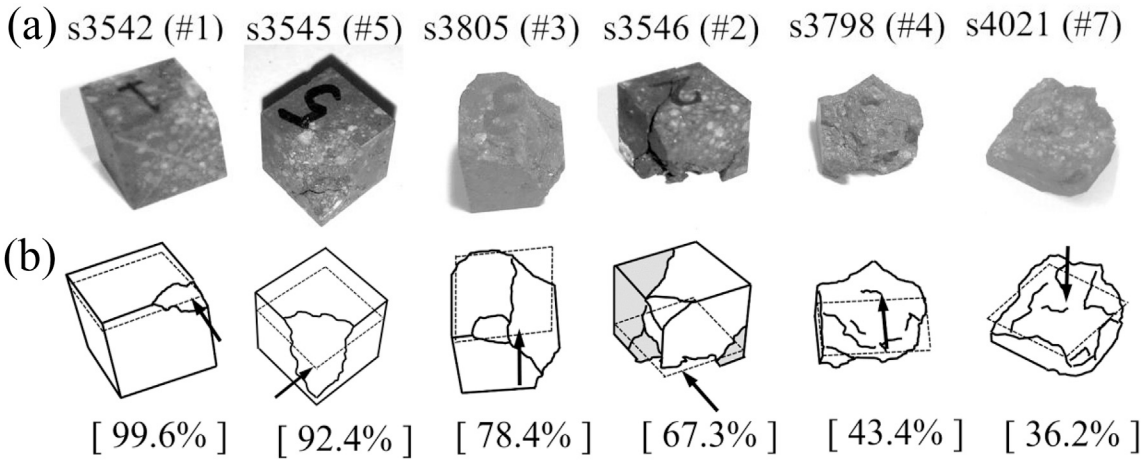

Fig. 4. Largest fragments after impacts. (a) Photographs of largest fragment in order of degree of target fragmentation, with shot numbers. The target numbers are given in parentheses. (b) Corresponding illustrations indicating fracture surfaces. The ratios of the mass of the largest fragments to the initial target mass (M_l/M_t) are given in square brackets. The trajectories of the projectiles are indicated in the direction of the arrow. The dotted square corresponds to the tomograms shown in Fig. 5. For shot s3546 (#2), the second, third and fourth largest fragments are shown as shaded parts to put them into the context of the cracks within the entire target.

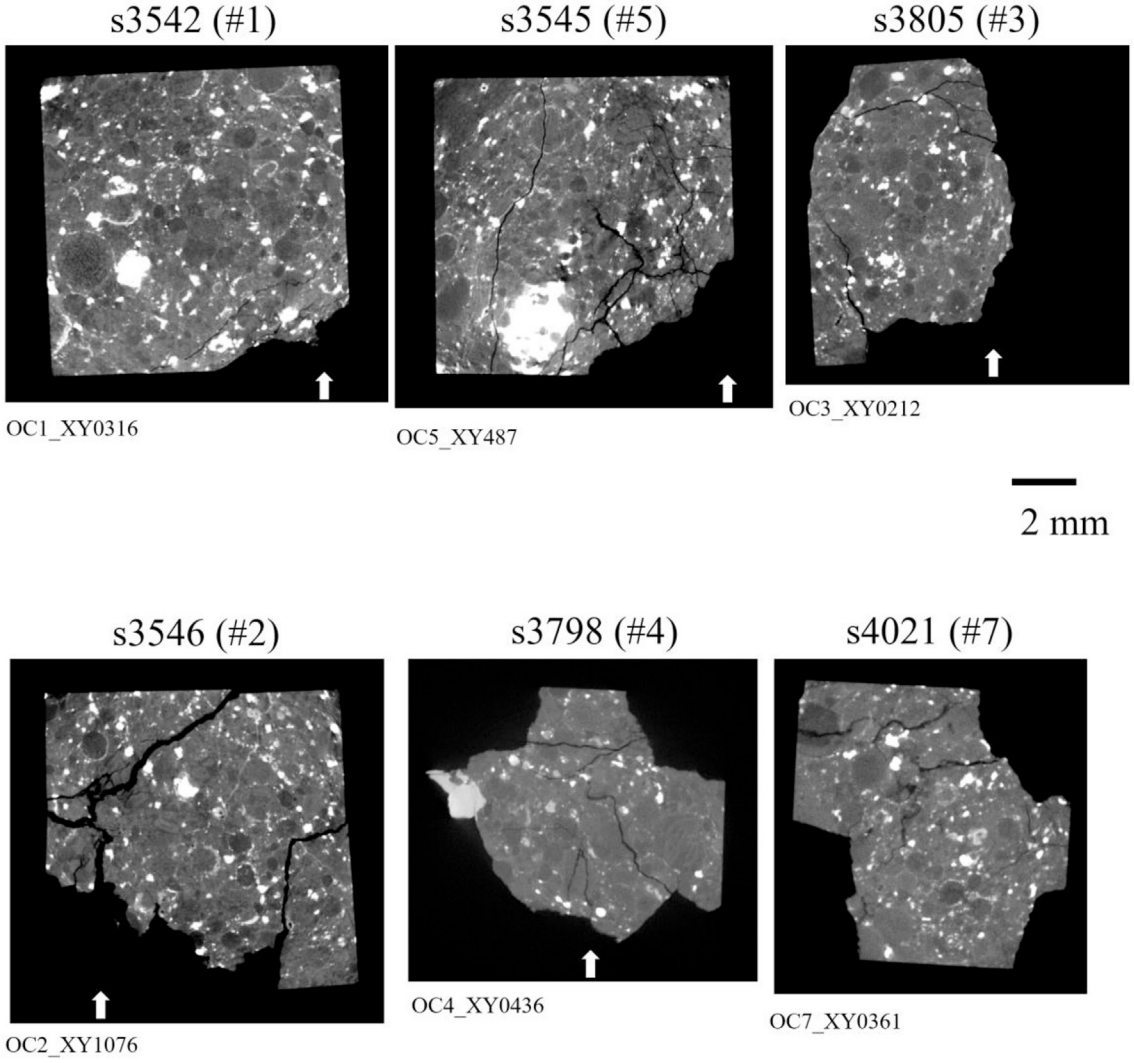

Fig. 5. Typical tomograms of largest fragments corresponding to the dotted square shown in Fig. 4. For shot s3546 (#2), the second, third and fourth largest fragments are measured. The trajectories of the projectiles are indicated in the direction of the arrow except for shot s4021. In shot s4021, the direction of the trajectory of the projectile is from the front to the back of the figure.

growth). Indeed, most cracks appear to grow regardless of the original large crack observed by X-ray microtomograph before the impact experiments at resolutions with 9.0 μm/voxel.

4.3. Crack growth in CTMA grains

CTMA grains with an impact-induced crack are investigated. Typical three-dimensional images of the grains of chondrules, produced using ImageJ, are shown in Fig. 8. The three-dimensional image is separated for two components: CTMA grain space and crack space. CTMA grain is divided by cracks. Then, the ratio of the volume of the largest fragment after impact (V_{lar}) to the original CTMA grain's volume before impact (V_{ori}) is investigated as an indicator of CTMA grain's fragmentation (From now on, we will refer to this volume ratio as "R"). That is, the heavier the degree of fragmentation, the lower the value of R becomes. The grayscale-based thresholding techniques is sensitive to small changes in the parameters used for segmentation. Small relative changes in the grayscale values selected result in absolute differences in measured volumes of CTMA grains. We estimate a 15% standard deviation for the corresponding error. However, the value of R remains almost constant (differences less than a few percentage), regardless of grayscale value because the relative volume is similar.

Based on the three-dimensional visualization of the crack growth in CTMA grains and the value of R, the crack growths are grouped into four patterns in this study.

Pattern I: Crack growth along the boundary surfaces of CTMA grains (CTMA grain boundaries from now on). The values of R range from 1 to 0.97. A value of 0.97 corresponds to the largest part's volume ratio when the sphere is cut parallel to its diameter by one tenth from the top (We assume the mineral grain's shape is spherical for simplicity).
Pattern II: Crack growth under CTMA grain boundaries. The values of R range from 0.97 to 0.84. The value of 0.84 corresponds to the largest part's volume ratio when the sphere is cut parallel to its diameter by one fourth from the top.
Pattern III: Crack growth through the center of CTMA grain. The values of R are less than 0.84.
Pattern IV: Multiple cracks emanating within CTMA grain. The values of R are less than 0.84.

Fig. 9 shows the above pattern of crack growth and each ratio for CTMA grains. In the experiments, some cracked CTMA grains were removed from the observation list because their boundaries were obscured. The observed numbers of CTMA grains with cracks are as follows (Table 1): Twenty-seven chondrules with cracks are observed for shot s3542 (#1), s3545 (#5), s3805 (#3) and s3798 (#4). Seventeen

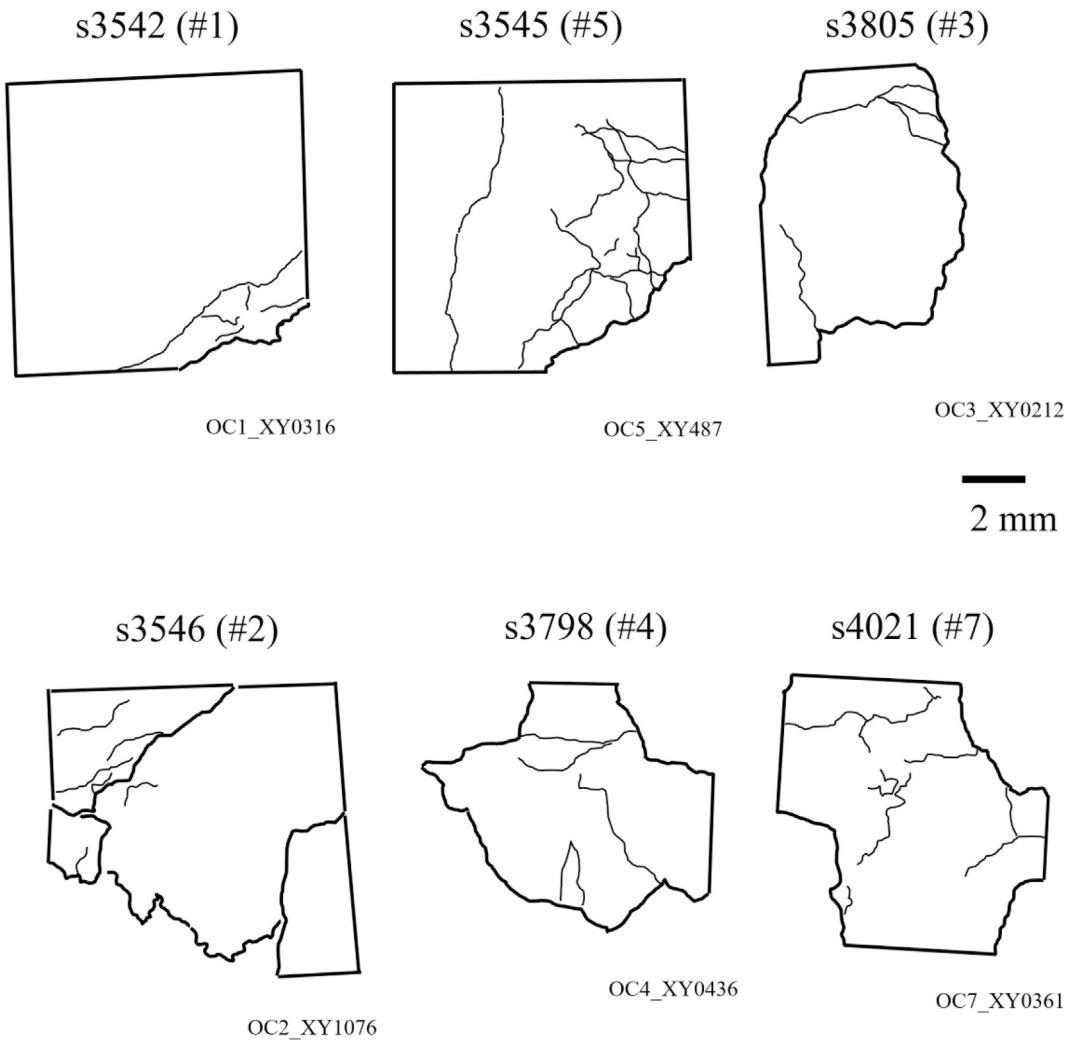

Fig. 6. Illustrations of main cracks within the fragments shown in the typical tomograms of Fig. 5.

troilites (FeS) with cracks are observed for shot s3545 (#5) and s3546 (#2). Ten aggregates of troilite and Fe-Ni metals are observed for s3545 (#5), s3805 (#3) and s3546 (#2). Twenty-seven Fe-Ni metals are observed for all shots.

In chondrules, the Pattern III and IV make up more than half of the observations, indicating that most cracks grow regardless of CTMA grain boundaries. On the other hand, in Fe-Ni metal, almost all cracks are Pattern I, indicating that almost all cracks grow along CTMA grain boundaries. In general, the strength of Fe-Ni metal is much higher than that of chondrules (and is both more elastic and more ductile than most minerals). The order of decreasing strength is presumably Fe-Ni metal, aggregates of troilite and Fe-Ni metal, troilite, and chondrules. In that case, the weaker the strength of CTMA grains, the more likely crack growth tends to occur regardless of CTMA grain boundaries.

Crack growth would be affected by the degree of shock loading from the impact point. To investigate the influence of the degree of shock loading on crack growth, the relationship between the distance from the impact point (the degree of shock loading generally decreases with increasing the distance from impact point) and the volume ratio of largest grain fragment R is given in Fig. 10. Except for chondrules, crack growth (R) appears to be unaffected by the distance from the impact point. For chondrules, cracks of Pattern I are not observed at distances less than 6 mm from the impact point, and there appears to be a weak correlation (the correlation coefficient is about 0.50) between the distance from impact point and R. In particular, for shot s3545, the value of R clearly decreases with decreasing distance from the impact point. This may suggest that the smaller the distance from the impact point (the stronger the degree of shock loading), the less likely crack growth is affected by CTMA grain boundaries. However, the amount of our data is insufficient to reveal the relationship between the distance from impact point and R for chondrules. Moreover, our targets are quite small and therefore unlikely to reliably reveal that relationship. We will discuss this in more detail in next section.

Chondrule tends to be larger in size than grains of troilite, aggregates of troilite and Fe-Ni metal, and Fe-Ni metal. In general, relatively large cracks exist in large grains even if the material is taken into account. For the same material, the size of CTMA grain alone may affect the degree of its fragmentation. To confirm this, the relationships between the grain's volume and R in chondrules and troilite (in the experiments, the average size of chondrules is largest and that of troilite is smallest) are shown in Fig. 11. In chondrules, the value of R appears to be independent of the grain's volume (the correlation coefficient is about 0.25). On the other hand, in troilite, the value of R appears to decrease with increasing volume (the correlation coefficient is about 0.62). However, to add another point of view, if we remove the largest troilite grain, the value of R appears to be independent of the grain's volume. As the amount of our data might be insufficient to reveal the relationship, further study is necessary to understand the relationship between grain size and degree of fragmentation.

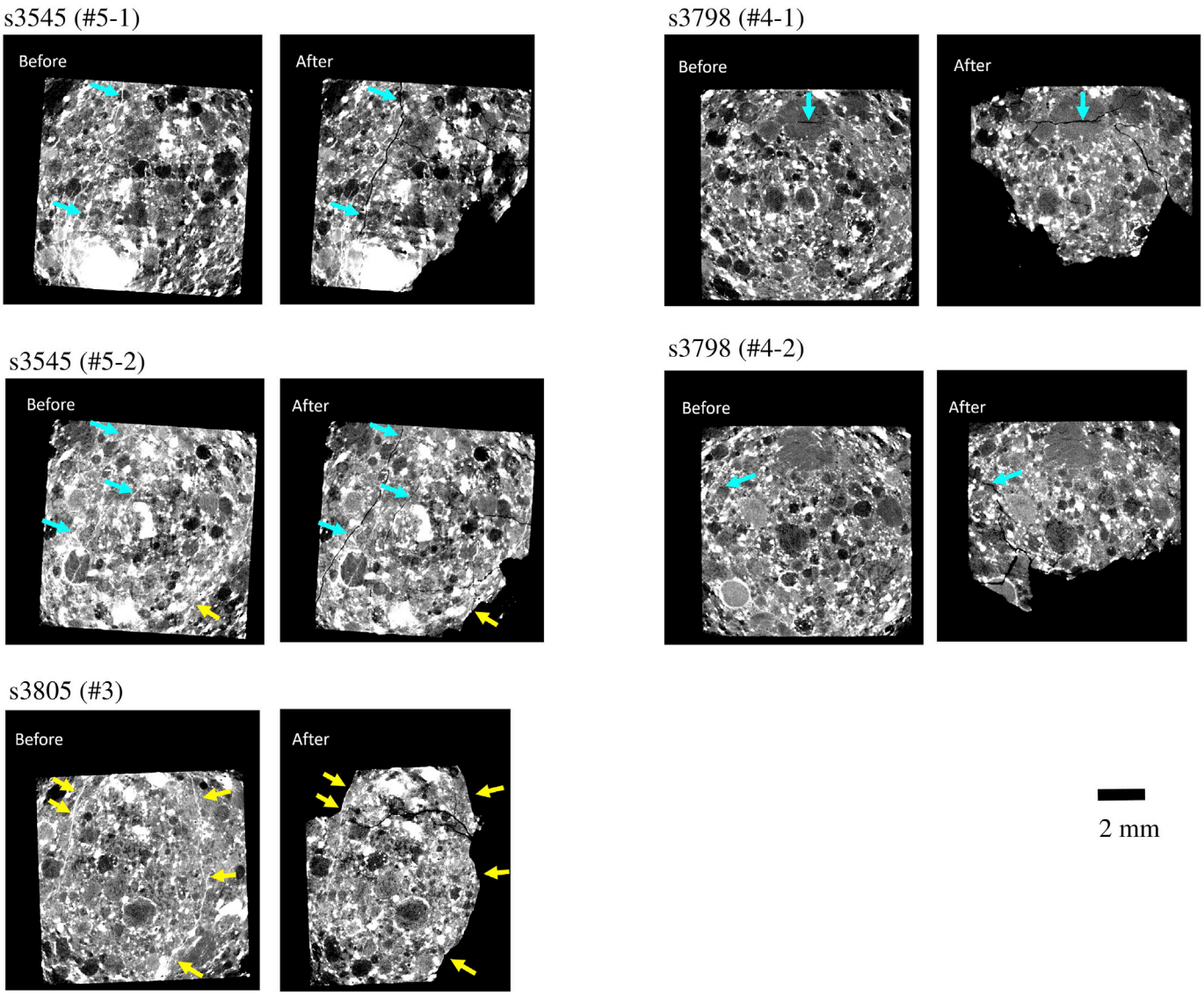

Fig. 7. All observed fracture surfaces as well as crack growth resulting from original cracks due to impacts. Yellow arrows mark fracture surfaces in the pictures before and after the impact. Light-blue arrows mark growing cracks in the pictures before and after the impact. The directions of projectiles' trajectories are from bottom to top in the figures. (For interpretation of the references to colour in this figure legend, the reader is referred to the Web version of this article.)

5. Discussion

5.1. Difference of crack growth within individual CTMA grains

The experimental results suggest that impact-induced crack growth within CTMA grains is affected by the grains' strength.

In ductile Fe-Ni metal grains, which are considered to be strongest among the observed CTMA grains, almost all cracks grow along their grain boundaries regardless of the degree of shock loading. Friedrich and Rivers (2013) investigated seven small chips of ordinary chondrites using high resolution (2.6 μm/voxel) synchrotron X-ray microtomography scans. They reported that no cracks or fractures are seen in Fe-Ni metal grains. The same result is obtained in our SEM images of the thin sections and X-ray microtomography scans for the L5 chondrites. According to Friedrich and Rivers (2013), Fe-Ni metal grains did experience the same impact event on the asteroid as the silicate material, but deformation rather than cracking was the result. Thus, as Fe-Ni metal grains have no micro-cracks, cracks would grow along the grain boundaries.

In chondrules, which are considered to be the weakest among the CTMA grains, most cracks grow regardless of chondrule grain boundaries. The reason is probably due to the existence of micro-cracks within the chondrules. These micro-cracks cannot be imaged by our X-ray microtomography at a resolution with 9.0 μm/voxel but can be identified using SEM images of thin sections (Fig. 1). These micro-cracks would induce the degradation of the chondrule grain's strength. Although crack growth mostly occurs regardless of grain boundaries, several cracks grow along grain boundaries. According to Friedrich and Rivers (2013), occasionally, pore space is visible as weak three-dimensional outlines around individual chondrules. In our SEM images of the thin sections and X-ray microtomography scans, apparent white outlines around individual chondrules are observed. These are considered to be hydroxide filling in the pore space. Crack growth along chondrule grain boundaries may occur when pore space around the grain already exists and the degree of shock loading is weak.

Crack growth in troilite seems to be similar to cracking in chondrules. Friedrich and Rivers (2013) pointed out that troilite grains do occasionally contain void spaces. Moreover, they suggested that voids in troilite grains may originate from a cooling process as troilite has a larger coefficient of thermal expansion than Fe-Ni metal. Therefore, the creation of these voids would degrade of troilite grains' strength and nearly

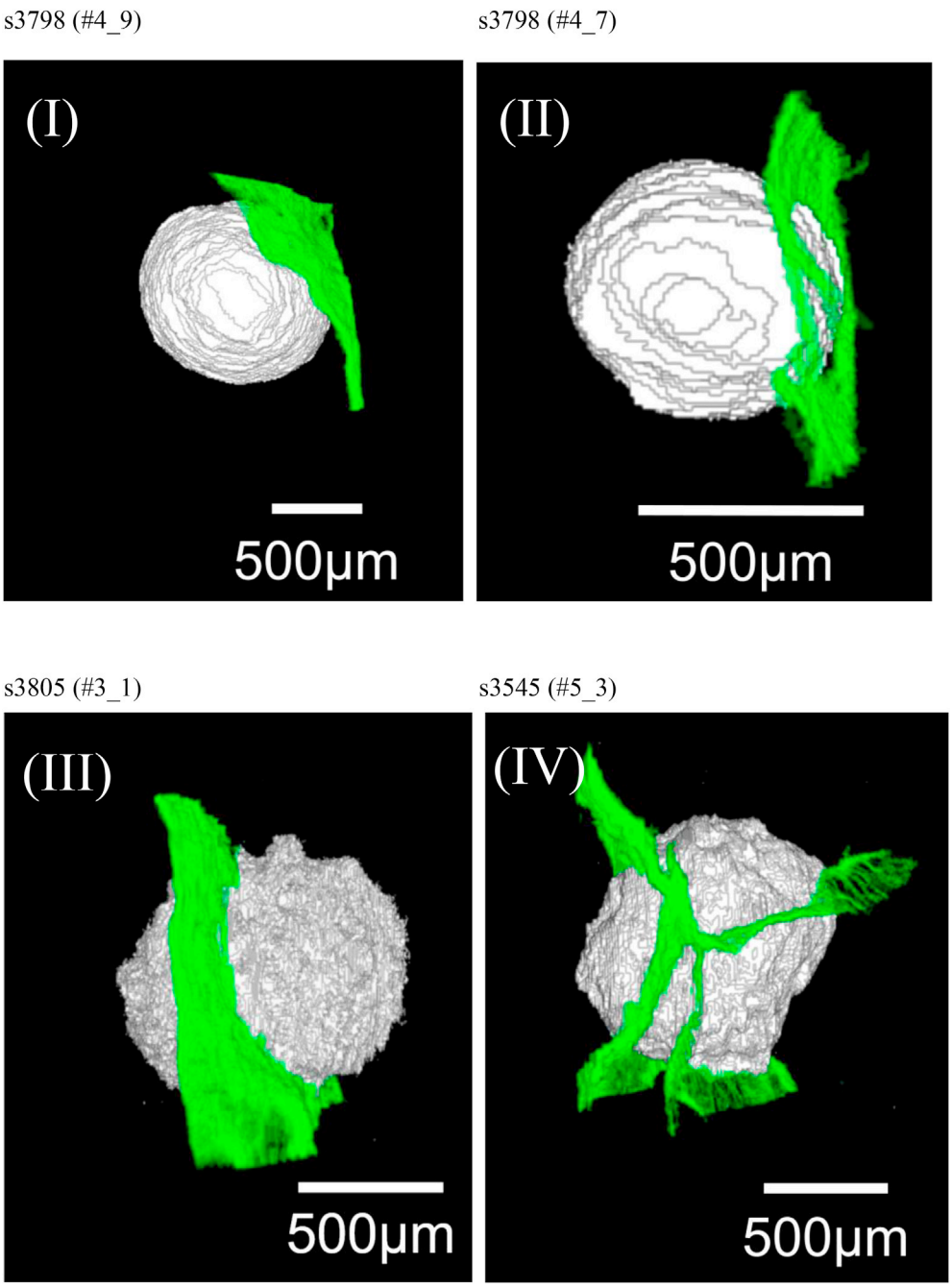

Fig. 8. Typical three-dimensional images of the grains of chondrules (shown in white) with impact-induced cracks (shown in green) for each pattern of crack growth. (I) Pattern I: crack growth along the boundary surface of the grain. (II) Pattern II: crack growth under the boundary surface of the grain. (III) Pattern III: crack growth through the center of the grain. (IV) Pattern IV: multiple cracks emanating within the grain. For more detailed explanation about each pattern, see text. (For interpretation of the references to colour in this figure legend, the reader is referred to the Web version of this article.)

half of cracks would grow through the centers of the grains.

From the experimental results, we cannot rule out the possibility that impact-induced crack growth within chondrules is affected by the degree of shock loading. In chondrules, the impact-induced cracks located near the impact point (which is considered to experience strong shock loading) appear to grow regardless of chondrule grain boundaries, while the impact-induced cracks located at the far side of the impact point (which is considered to experience relatively weak shock loading) appear to grow along chondrule grain boundaries. However, a strong correlation between the distance from the impact point and the volume ratio of largest grain fragment R is not observed in the experiments although the degree of shock loading is expected to be decreases with increasing the distance from the impact point. For a plausible explanation, we think that the degree of shock loading is not a function of the distance from the impact point in our experiments because of our targets were small compared to the projectile. The high pressure in a shock wave is relieved by the propagation of a rarefaction wave. This rarefaction wave, which is the reflection of the shock wave, consequently causes the crack growth in the target. If the target size were much larger than the projectile, the intensity of rarefaction waves (which are originating from the back sides of the projectile and the target) would decrease with increasing distance from the impact point. If the target size is not much larger than the projectile, multiple rarefaction waves originating from several target surfaces occur and the development of rarefaction waves is much more complicated. As a result, the intensity of rarefaction waves may almost never change in the target. In that case, the intensity of rarefaction would be not a function of distance from the impact point.

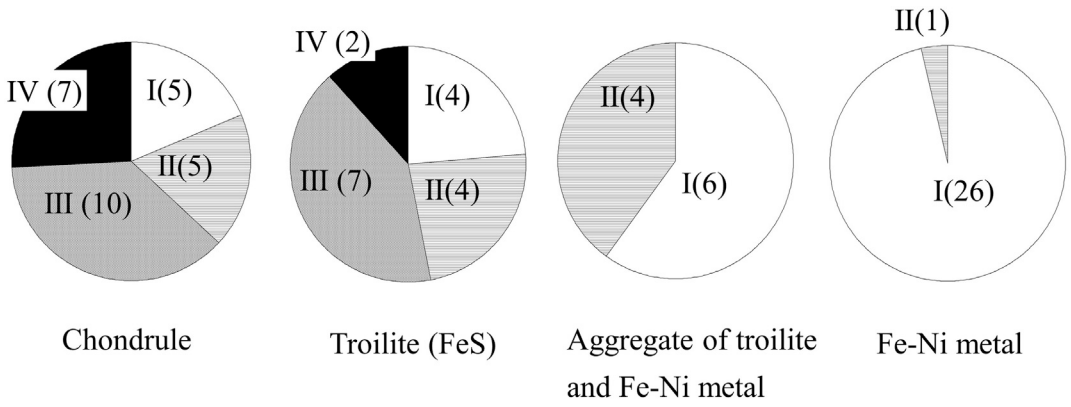

Fig. 9. Proportion of crack growth by pattern type for chondrule, troilite, aggregates of troilite and Fe-Ni metal, and Fe-Ni metal. The definition of each pattern is indicated in Fig. 8. The number of each pattern is given in parentheses.

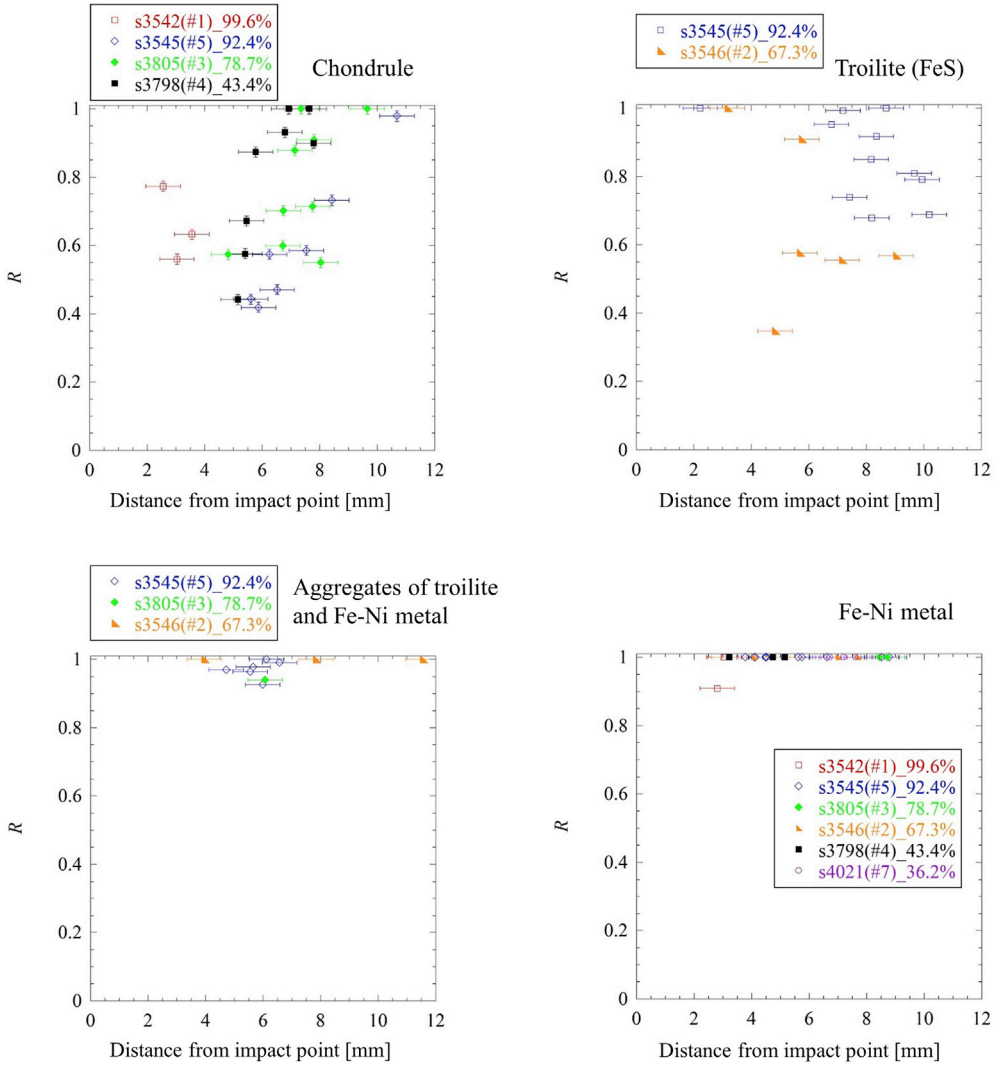

Fig. 10. Distance from impact point vs *R* (the ratio of the volume of the largest grain fragment after impact (V_{lar}) to the volume of the original mineral grain before impact (V_{ori})). Standard errors are indicated. With the exception of chondrules, the vertical error bars are smaller than the corresponding symbol sizes.

5.2. Implication for Itokawa particles

The experimental results show that, in the case of impacts, crack growth regardless of chondrule grain boundaries is a dominant pattern whereas the crack growth along chondrule grain boundaries is a minor pattern. The opposite is considered to be the case for crack growth in thermal fatigue. For instance, Richter and Simmons (1974) performed thermal cycling experiments for basalt targets and suggested that rapid rates of temperature change induce crack growth along grain boundaries due to mismatches in thermal expansion coefficients of the component minerals.

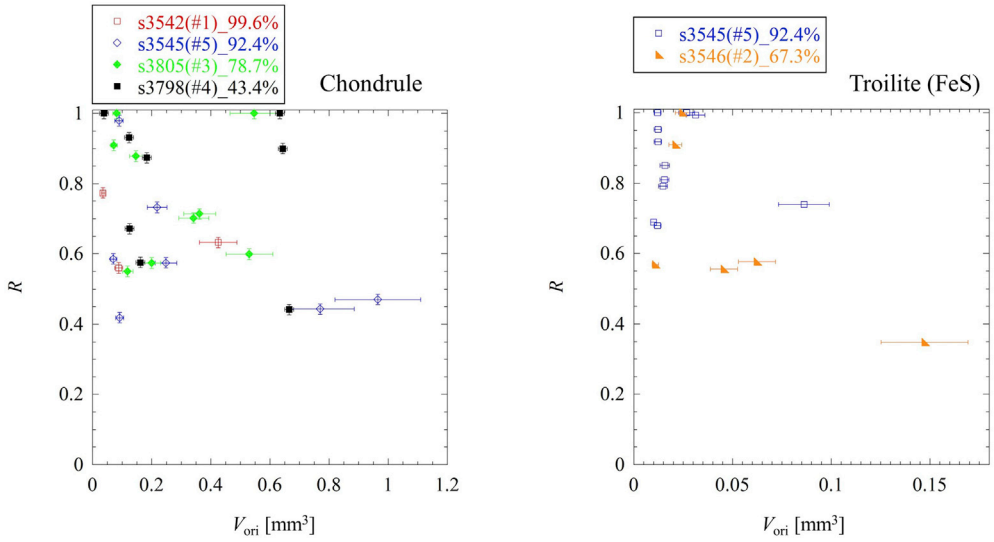

Fig. 11. V_{ori} vs $R(=V_{ori}/V_{lar})$ only for chondrule and troilite with standard errors. The error bars of vertical axis except for chondrule are smaller than the size of each symbol.

It is noted that we do not rule out the possibility of crack growth within chondrules by thermal fatigue because the experimental data available of thermal fatigue for chondrules are insufficient at the time of writing and the chondrules consist of several mineral constituent grains. The differences in the thermal expansion coefficients among the mineral constituent grains within chondrules are considered to be smaller than between the chondrules and their surrounding recrystallized matrix. This is because the material differences among the mineral constituent grains within chondrules are smaller than between the chondrules and their surrounding recrystallized matrix. Therefore, we suppose that, if thermal fatigue induces the crack growth within a chondrule, it also strongly induces the crack growth along the chondrule grain boundary.

The sizes of Itokawa regolith particles recovered by the Hayabusa mission ranges from sub-micrometer to a hundred micrometers (note that, in order to apply our results to asteroid Itokawa, it is necessary to understand the difference between Itokawa particles and asteroid Itokawa because the sizes of Itokawa particles are smaller than the CTMA grains. We discuss the topic in Appendix B). Tsuchiyama et al. (2011, 2014) have examined the three-dimensional microstructure of 48 Itokawa regolith particles with sizes from 13.5 to 114.3 μm using synchrotron radiation (SR)-based microtomography at SPring-8. The shape distribution of the Itokawa particles is similar to that of analogue impact fragments (Michikami et al., 2018). Their shape distributions of polymineralic and monomineralic particles are similar (Tsuchiyama et al., 2011, 2014).

Michikami et al. (2018) carried out impact experiments on an L5 chondrite, identical to the samples used in this study, and measured more than 500 tiny fragments with diameters of 46 μm–612 μm by synchrotron radiation-based microtomography at Spring-8. The shape distributions of the L5 chondrite's tiny fragments are similar to relatively larger impact fragments in catastrophic disruptions (e.g. the impact fragments ≥4 mm of basalts in Michikami et al., 2016). Any intact chondrules which separated from the rest of the material by impacts could neither be observed in Michikami et al.'s (2018) experiments nor this experiment although Flynn and Durda (2004) found some of these in impact experiments on ordinary chondrules. Michikami et al. (2018) suggested that the Itokawa particles are not the products of thermal fatigue but impact fragments on the asteroid surface.

Our experimental results imply that, in the case of impacts, most surfaces of relatively large fragments originating from chondrules do not contain their boundary surfaces because crack growth along the chondrule grain boundary is a minor pattern. To the contrary, in the case of thermal fatigue, most surfaces of relatively large fragments originating from the chondrules may contain their boundary surfaces because the crack growth along the chondrule grain boundary is considered to be a dominant pattern. For example, we consider a spherical target to approximate the shape of a chondrule. Michikami et al. (2016) carried out impact experiments on a spherical basalt target. The experimental result shows that the ten largest fragments in terms of mass are more spherical because their surfaces contain the curved surfaces of the original target. Their shapes are different from smaller impact fragments.

If relatively large Itokawa particles were produced by thermal fatigue, their shape distribution should be influenced by chondrule grain boundaries and deviate from that of relatively large impact fragments. However, the shapes of relatively large Itokawa particles with sizes of ~100 μm are similar to the shapes of relatively large impact fragments (see Table 1 in Tsuchiyama et al., 2014). Therefore, the experimental results of crack growth regardless of chondrule grain boundaries strongly support the hypothesis that Itokawa particles have not been produced by thermal fatigue and are likely to be impact fragments on the asteroid surface, as described in previous papers (Tsuchiyama et al., 2011, 2014; Michikami et al., 2018).

6. Conclusions

We have investigated three-dimensional imagery of impact-induced crack growth in L5 chondrites using X-ray microtomography at a resolution with the voxel size of 9.0 μm. Impact experiments for 9 mm side length cubic targets of L5 chondrites were performed using a two-stage light-gas gun at ISAS, JAXA. A spherical alumina projectile with 1.0 mm in diameter was shot perpendicularly into the target surface at a nominal impact velocity of 2.0 km/s. In a total of six successful impact experiments we have measured the following constituents of chondrites with cracks: twenty-seven type I chondrules, seventeen troilites (FeS), ten aggregates of troilite and Fe-Ni metals, and twenty-seven Fe-Ni metals. In chondrules and troilites, most cracks grow regardless of grain boundaries. On the other hand, in Fe-Ni metal, almost all cracks grow along grain boundaries. We predict that the weaker the strength of grains, the more likely crack growth tends to occur regardless of the grain boundaries. Based on our experimental results and previous studies for Itokawa particles and the shapes of laboratory impact fragments (Tsuchiyama et al., 2011, 2014; Michikami et al., 2018), we conclude that the Itokawa particles are not the products of thermal fatigue but impact fragments on Itokawa's surface.

Acknowledgments

We acknowledge Professor. H. C. Connolly of Rowan University for useful comments and Mr. T. Kadokawa for the support of the experiments. This study was supported by the Hypervelocity Impact Facility (former facility name: the Space Plasma Laboratory), ISAS, JAXA. We thank two anonymous referees for their careful review of the manuscript and their constructive comments. A.H. was supported by STFC grant no. ST/S001271/1. A. Tsuchiyama was supported by a Grant-in-Aid for Specially Promoted Research of the Japan Ministry of Education, Culture, Sports, Science and Technology (15H05695).

Appendix. ASupplementary data

Supplementary data to this article can be found online at https://doi.org/10.1016/j.pss.2019.07.005.

Appendix A. Investigation of the difference in experimental results between samples with and without target holders.

In order to investigate the difference in experimental results between samples with and without target holders, the basalt target samples adopted in previous laboratory impact experiments by Michikami et al. (2016, 2018), are used instead of L5 chondrites. This is because a large block is necessary to accurately fire the projectiles into the targets and the basalt targets are no less appropriate as mechanical analogs for asteroids than the materials used in previous experiments. The target bulk density is 3000 kg/m^3, the compressive strength is 185 MPa, and the tensile strength is 14 MPa (obtained from a cylinder splitting test).

Two impact experiments for cubic basalt targets (side length 4 cm) with and without target holders were carried out with a two-stage light gas gun at ISAS, JAXA. In each run, spherical nylon projectiles 7.14 mm in diameter (mass 0.219 g and density 1150 kg/m^3) were shot perpendicularly into the target surface at an impact velocity of 2.0 km/s. The projectile mass, target mass and the impact velocity are chosen to be the same as the specific energy Q of the experiments for L5 chondrites, where Q is the kinetic energy of the projectile per unit target mass.

In shot s3547, the target (mass 192.7 g) was enclosed in an aluminum target holder (mass 64.2 g) consisting of a 4 mm thick aluminum plate and only the front surface was exposed on the impact side. In shot s3548, the aluminum target holder was removed from the target (mass 195.1 g). Each target was set on a cylindrical stand less than one third of the target size in diameter. The whole system was mounted in a vacuum chamber (almost $1 \times 1 \times 2$ m^3) with acrylic resin windows. A cardboard box ($59 \times 56 \times 45$ cm^3) was put on the floor of the chamber to prevent the destruction of fast fragments by secondary collisions on the interior. The ambient pressure was less than 20 Pa. The setup of two high-speed framing camera was as before.

Each impact position is similar to that of shot s3545 and thus a side of each target is heavily broken. After each impact, all fragments are collected in the cardboard box. Fig. A1 shows the cumulative mass distributions of fragments for basalt target samples. In the experiments, several large fragments greater than 3 g in mass and many fine fragments smaller than 3 g originating from the heavily broken target's sides are observed. The total number of fragments in shot s3547 with a target holder is smaller than that in shot s3548 without a target holder. The reason for this is that part of the impact energy in shot s3547 is consumed by the target holder, which is bent modification near the corner. However, the s3547 and s3548 are very similar in terms of the space distributions of the fracture surfaces when several large fragments are piled up (Fig. A2). This means that s3547 and s3548 show a very similar behavior in terms of growth of relatively large cracks during impacts. Therefore, we assume that the target holder does not affect the growth of relatively large cracks during impacts. The difference between the experimental results for the targets with and without target holders can be assumed to be negligible, at least from the point of view of growth of relatively large cracks.

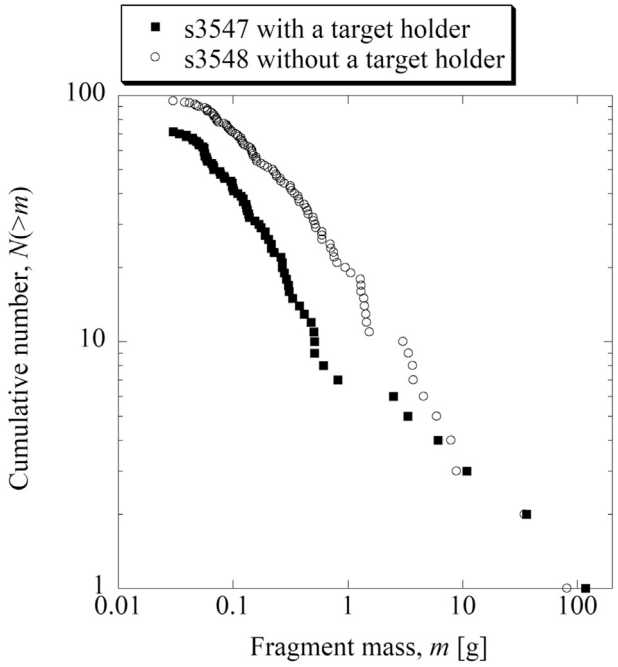

Fig. A1. Mass distributions of fragments for our experiments with basalt targets.

s3547 with a target holder s3548 without a target holder

Fig. A2. Several large fragments piled up originating from the impact experiments for the basalt targets with a target holder (left; s3547) and without a target holder (right; s3548). The side length of the original cubic target is 4 cm.

Appendix B. Difference between Itokawa particles and asteroid Itokawa

In this study, we focused on the relationship between CTMA grains and crack growth caused by impacts using an L5 chondrite as analogue material for Itokawa particles. The bulk density of the L5 chondrite is 3400 kg/m^3, the same as the Itokawa particles. However, the bulk density and the porosity of the Itokawa particles are different from those of asteroid Itokawa. As mentioned before, asteroid Itokawa's bulk density is low (1950 ± 140 kg/m^3; Abe et al., 2006) and its bulk porosity is high (~40%; Abe et al., 2006) based on the grain density of LL ordinary chondrites. Therefore, we have to understand the difference between Itokawa particles and asteroid Itokawa in order to apply the experimental results to asteroid Itokawa.

Much of the porosity in ordinary chondrites is in the form of void spaces between the grains. We cannot know the void spaces between the grains in the pebbles, cobbles and boulders on the surface of Itokawa because the Itokawa particles collected are smaller than individual chondrules. If these pebbles, cobbles and boulders have large void spaces, these would affect the crack growth of the chondrules caused by impacts. Meteorite impacts onto the asteroid surface induce the compaction of these void spaces (e.g. Friedrich and Rivers, 2013) which attenuate the shock loading during impacts.

The attenuation of the shock loading during impacts also induces a large amount of ejecta with low velocities (e.g. Michikami et al., 2007) and as a result a large amount of ejecta can accumulate on the asteroid surface. In general, the densities of ordinary chondrites fallen on the Earth are high while their porosities are low compared with asteroid Itokawa. Recently, Flynn et al. (2018) reported the velocities of crater ejecta produced by hypervelocity impacts on the L3-6 ordinary chondrites NWA 869 and showed that most of the crater ejecta have velocities larger than a few m/s, while the escape velocity on Itokawa is 0.20 m/s (e.g. Michikami et al., 2008). This suggests that almost all crater ejecta escape from Itokawa if their densities and porosities are similar to ordinary chondrites fallen on the Earth.

As can be seen above, the impact experiments for chondrites with low density and high porosity are necessary to investigate the influence of the porosity on crack growth within a chondrule and ejecta velocity. However, such samples never exist as chondrites on the Earth. In the future, instead of such chondrites, we can only carry out the impact experiments on artificial analogue samples with low density and high porosity.

References

Abe, S., Mukai, T., Hirata, N., Barnouin-Jha, O.S., Cheng, A.F., Demura, H., Gaskell, R.W., Hashimoto, T., Hiraoka, K., Honda, T., Kubota, T., Matsuoka, M., Mizuno, T., Nakamura, R., Scheeres, D.J., Yoshikawa, M., 2006. Mass and local topography measurements of Itokawa by Hayabusa. Science 312, 1344–1347.

Britt, D.T., Yeomans, D., Housen, K., Consolmagno, G., 2002. Asteroid Density, Porosity, and Structure, Asteroid III. Univ of Arizona Press, Tucson, pp. 485–500.

Delbo, M., Libourel, G., Wilkerson, J., Murdoch, N., Michel, P., Ramesh, K.T., Ganino, C., Verati, C., Marchi, S., 2014. Thermal fatigue as the origin of regolith on small asteroids. Nature 508, 233–236. https://doi.org/10.1038/nature13153.

Flynn, G.J., Durda, D.D., 2004. Chemical and mineralogical size segregation in the impact disruption of inhomogeneous, anhydrous meteorites. Planet. Space Sci. 52, 1129–1140.

Flynn, G.J., Durda, D.D., Patmore, E.B., Jack, S.J., Molesky, M.J., May, B.A., Congram, S.N., Strait, M.M., Macke, R.J., 2018. Hypervelocity cratering and disruption of the Northwest Africa 869 ordinary chondrite meteorite: Implications for crater production, catastrophic disruption, momentum transfer and dust production on asteroids. Planet. Space Sci. 164, 91–105.

Friedrich, J.M., Wignarajah, D.P., Chaudhary, S., Rivers, M.L., Nehru, C.E., Ebel, D.S., 2008. Three-dimensional petrography of metal phases in equilibrated L chondrites—effects of shock loading and dynamic compaction. Earth Planet. Sci. Lett. 275, 172–180.

Friedrich, J.M., Rivers, M.L., 2013. Three-dimensional imaging of ordinary chondrite microporosity at 2.6 μm resolution. Geochim. Cosmochim. Acta 116, 63–70.

Fujiwara, A., Kamimoto, G., Tsukamoto, A., 1977. Destruction of basaltic bodies by high-velocity impact. Icarus 31, 277–288.

Fujiwara, A., Kawaguchi, J., Yeomans, D.K., Abe, M., Mukai, T., Okada, T., Saito, J., Yano, H., Yoshikawa, M., Scheeres, D.J., Barnouin-Jha, O., Cheng, A.F., Demura, H., Gaskell, R.W., Hirata, N., Ikeda, H., Kominato, T., Miyamoto, H., Nakamura, A.M., Nakamura, R., Sasaki, S., Uesugi, K., 2006. The rubble-pile asteroid Itokawa as observed by Hayabusa. Science 312, 1330–1334.

Housen, K.R., Wilkening, L.L., Chapman, C.R., Greenberg, R., 1979. Asteroidal regoliths. Icarus 39, 317–351.

Hutchison, R., 2004. Meteorites: A Petrologic, Chemical and Isotopic Synthesis. Cambridge University Press, Cambridge, UK, p. 506.

Kawai, N., Tsurui, K., Hasegawa, S., Sato, E., 2010. Single microparticle launching method using two-stage light-gas gun for simulating hypervelocity impacts of micrometeoroids and space debris. Rev. Sci. Instrum. 81, 115105.

Medvedev, R.V., Gorbatsevich, F.I., Zotkin, I.T., 1985. Determination of the physical properties of stony meteorites with application to the study of processes of their destruction. Meteoritika (in Russian) 44, 105–110.

Michikami, T., Moriguchi, K., Hasegawa, S., Fujiwara, A., 2007. Ejecta velocity distribution for impact cratering experiments on porous and low strength targets. Planet. Space Sci. 55, 70–88.

Michikami, T., Nakamura, A.M., Hirata, N., Gaskell, R.W., Nakamura, R., Honda, T., Honda, C., Hiraoka, K., Saito, J., Demura, H., Ishiguro, M., Miyamoto, H., 2008. Size-

frequency statistics of boulders on global surface of asteroid 25143 Itokawa. Earth Planets Space 60, 13–20.
Michikami, T., Hagermann, A., Kadokawa, T., Yoshida, A., Shimada, A., Hasegawa, S., Tsuchiyama, A., 2016. Fragment shapes in impact experiments ranging from cratering to catastrophic disruption. Icarus 264, 316–330.
Michikami, T., Kadokawa, T., Tsuchiyama, A., Hagermann, A., Nakano, T., Uesugi, K., Hasegawa, S., 2018. Influence of petrographic textures on the shapes of impact experiment fine fragments measuring several tens of microns: Comparison with Itokawa regolith particles. Icarus 302, 109–125.
Mikouchi, T., Miyamoto, M., McKay, G.A., 2001. Mineralogy and petrology of the Dar al Gani 476 martian meteorite: Implications for its cooling history and relationship to other shergottites. Meteorit. Planet. Sci. 36, 531–548.
Molaro, J.,L., Byrne, S., Langer, S.,A., 2015. Grain-scale thermoelastic stresses and spatiotemporal temperature gradients on airless bodies, implications for rock breakdown. J. Geophys. Res. Planets 120, 255–277. https://doi.org/10.1002/2014JE004729.
Nakamura, A., Fujiwara, A., 1991. Velocity distribution of fragments formed in a simulated collisional disruption. Icarus 92, 132–146.
Nelson, V.E., Rubin, A.E., 2002. Size-frequency distributions of chondrules and chondrule fragments in LL3 chondrites: Implications for parent-body fragmentation of chondrules. Meteorit. Planet. Sci. 37, 1361–1376.
Okumura, S., Sasaki, O., 2014. Permeability reduction of fractured rhyolite in volcanic conduits and its control on eruption cyclicity. Geology 42 (10), 843–846.
Richter, D., Simmons, G., 1974. Thermal expansion behavior of igneous rocks. Int. J. Rock Mech. Min. Sci. Geomech. Abstr. 11, 403–411.
Righter, K., Abell, P., Agresti, D., Berger, E.L., Burton, A.S., Delaney, J.S., Fries, M.D., Gibson, E.K., Haba, M.K., Harrington, R., Herzog, G.F., Keller, L.P., Locke, D., Lindsay, F.N., McCoy, T.J., Morris, R.V., Nagao, K., Nakamura-Messenger, K., Niles, P.B., Nyquist, L.E., Park, J., Peng, Z.X., Shih, C.-Y., Simon, J.I., Swisher, C.C., Tappa, M.J., Turrin, B.D., Zeigler, R.A., 2015. Mineralogy, petrology, chronology, and exposure history of the Chelyabinsk meteorite and parent body. Meteorit. Planet. Sci. 50, 1790–1819.
Saito, J., Miyamoto, H., Nakamura, R., Ishiguro, M., Michikami, T., Nakamura, A.M., Demura, H., Sasaki, S., Hirata, N., Honda, C., Yamamoto, A., Yokota, Y., Fuse, T., Yoshida, F., Tholen, D.J., Gaskell, R.W., Hashimoto, T., Kubota, T., Higuchi, Y., Nakamura, T., Smith, P., Hiraoka, K., Honda, T., Kobayashi, S., Furuya, M., Matsumoto, N., Nemoto, E., Yukishita, A., Kitazato, K., Dermawan, B., Sogame, A., Terazono, J., Shinohara, C., Akiyama, H., 2006. Detailed images of asteroid 25143 Itokawa from Hayabusa. Science 312, 1341–1344.
Tsuchiyama, A., Uesugi, K., Nakano, T., Ikeda, S., 2005. Quantitative evaluation of attenuation contrast of X-ray computed tomography images using monochromatized beams. Am. Mineral. 90, 132–142.
Tsuchiyama, A., Uesugi, M., Matsushima, T., Michikami, T., Kadono, T., Nakamura, T., Uesugi, K., Nakano, T., Sandford, S.A., Noguchi, R., Matsumoto, T., Matsuno, J., Nagano, T., Imai, Y., Takeuchi, A., Suzuki, Y., Ogami, T., Katagiri, J., Ebihara, M., Ireland, T.R., Kitajima, F., Nagao, K., Naraoka, H., Noguchi, T., Okazaki, R., Yurimoto, H., Zolensky, M.E., Mukai, T., Abe, M., Yada, T., Fujimura, A., Yoshikawa, M., Kawaguchi, J., 2011. Three-dimensional structure of Hayabusa samples: Origin and evolution of Itokawa regolith. Science 333, 1125–1128.
Tsuchiyama, A., Uesugi, M., Uesugi, K., Nakano, T., Noguchi, R., Matsumoto, T., Matsuno, J., Nagano, T., Imai, Y., Shimada, A., Takeuchi, A., Suzuki, Y., Nakamura, T., Noguchi, T., Abe, M., Yada, T., Fujimura, A., 2014. Three-dimensional microstructure of samples recovered from asteroid 25143 Itokawa: Comparison with LL5 and LL6 chondrite particles. Meteorit. Planet. Sci. 49, 172–187.
Villeneuve, J., Libourel, G., Soulié, C., 2015. Relationships between type I and type II chondrules: implications on chondrule formation processes. Geochim. Cosmochim. Acta 160, 277–305.
Yano, H., Kubota, T., Miyamoto, H., Okada, T., Scheeres, D., Takagi, Y., Yoshida, K., Abe, M., Abe, S., Barnouin-Jha, O., Fujiwara, A., Hasegawa, S., Hashimoto, T., Ishiguro, M., Kato, M., Kawaguchi, J., Mukai, T., Saito, J., Sasaki, S., Yoshikawa, M., 2006. Touchdown of the Hayabusa spacecraft at the Muses Sea on Itokawa. Science 312, 1350–1353.
Yomogida, K., Matsui, T., 1983. Physical properties of ordinary chondrites. J. Geophys. Res. 88, 9513–9533.